Sub-Mesoscale Eddy Detection from Sentinel-1A SAR Image: A Case Study Along Vizag Coast

Maria Sansanna, Lekshmi S., P.A. Maheswaran* and Praveen Naresh

DRDO-Naval Physical Oceanographic Laboratory, Kochi - 682 021, India *E-mail: maheswaran.npol@gmail.com

ABSTRACT

Oceanic eddies are important ocean surface features and play a crucial role in ocean energy transfer, nutrient distribution and biological production in the global ocean. Sub-mesoscale eddies are characterized by their small spatial scales (<100km) and short temporal scales (hours to days). Large mesoscale eddies are detected using satellite altimetry data where as sub-mesoscale eddies are detected using Synthetic Aperture Radar(SAR) images of high resolution. This paper analyses two such eddies captured in a SAR image off the coast of Vizag. The SAR image is despeckled and thresholded to extract the eddy features. The eddy images are analysed and validated using Sea Level Anomaly(SLA) and Chlorophyll-a datasets in order to understand the eddy dynamics and its characteristics.

Keywords: Synthetic Aperture Radar (SAR); Sub-mesoscale eddy; Sea Level Anomaly (SLA)

1. INTRODUCTION

Oceanic eddies, characterized by coherent vortices of water are prevalent features across the world oceans, ranging from tens to thousands of kilometers in diameters¹⁻². Submesoscale eddies are eddies with dimensions smaller than the baroclinic Rossby radius of deformation3. They affect horizontal mixing in the ocean (in particular, redistributing surface/subsurface pollution), marine biological population and other physical properties, like temperature and salinity⁴. The formation of sub-mesoscale eddies is often attributed to barotropic-baroclinic instabilities in oceanic fronts and currents⁵⁻⁶. Baroclinic instabilities arise due to the presence of a vertical shear in the ocean's velocity field, associated with density gradients due to temperature and salinity variations. These instabilities can lead to the growth of perturbations that evolve into coherent eddies. Barotropic instability on the other hand is driven by the horizontal shear in the ocean currents, leading to the formation of vortices when the flow becomes unstable. These instabilities are particularly prominent in regions with strong frontal gradients, such as boundary currents, upwelling zones and areas with significant temperature and salinity contrasts^{7-8.}

Satellite altimetry has been instrumental in identifying and tracking mesoscale eddies, however when it comes to tracking small scale eddies, there is a need for remote sensing data with enhanced spatial resolution⁹⁻¹⁰. Synthetic Aperture Radar (SAR) emerges as a preferred sensor due to its ability to provide high-resolution imagery and sensitivity to radar signals¹¹. The ocean surface roughness responsible for backscattering energy detected by radar is mainly due to the capillary and small gravity waves generated by the local wind¹². SAR's capability

Received: 01 May 2025, Revised: 31 July 2025

Accepted: 12 September 2025, Online published: 04 November 2025

to capture oceanic eddy details independent of weather or time of day makes it an important tool for eddy detection.

Bay of Bengal (BoB) is a semi-enclosed tropical region in the North-Eastern Indian Ocean, which is distinguished by its significant geographical and hydrological features. Bounded by India, Bangladesh, Myanmar, and the Andaman and Nicobar Islands, the bay is characterized by a large influx of freshwater from major rivers like the Ganges, Brahmaputra, and Irrawaddy, leading to pronounced stratification in its water column¹³⁻¹⁴. This stratification results in a low-salinity surface layer to overlay a more saline deeper layer, which profoundly impacts the bay's circulation patterns and biological productivity¹⁵.

Additionally, BoB experiences substantial precipitation, particularly during the southwest monsoon (June to September), which further influences its freshwater input and stratification¹⁶⁻¹⁷ The East Indian Coastal Current (EICC) which is the western boundary current of BoB, reverses twice a year in response to the seasonal reversal of monsoon winds¹⁸. It flows north eastward from February to September and south-westward from October to January. In March, a transitional period between the monsoon phases, EICC typically strengthens, flowing poleward joining the basin wide anticyclonic gyre¹⁸. This complex interplay of freshwater influx, precipitation, and seasonal current reversals makes BoB a significant area for oceanographic and climate studies.

The cyclonic (anticyclonic) eddy induced upwelling (downwelling) will bring sufficient (deficient) nutrients from the subsurface and increase (decrease) the productivity greatly¹⁹⁻²⁰.

Eddies can be recognized in SAR images as dark, narrow, curvilinear, and concentric bands (slicks) that appear to spiral inward or by a narrow band of increased brightness, usually related to current shear.

In this study, two sub-mesoscale eddies that were simultaneously observed in a SAR image near the North-Western BoB, are analysed. The image was captured on 13th March 2023, during which the EICC flows poleward. The SAR image has been processed, and a comparison with altimetry and chlorophyll data has been conducted.

2. METHODOLOGY

The SAR image was taken from Alaska Satellite Facility (ASF) which is part of the Geophysical Institute of the University of Alaska Fairbanks. It operates the NASA archive of SAR data and provides services to researchers. The images were obtained using Sentinel – 1 A, which carries C-band SAR instrument. The image is a Level 1 product, Ground Range Detection (GRD) image. It is dual polarized (VV & VH) with an interferometric wide beam and 250 km swath width.



Figure 1. Footprint of the original SAR image captured on 13th March, 2023; overlaid over the world map.

Among the various polarization modes, vertical (V) polarization is often favoured over horizontal (H) polarization for oceanic studies due to its higher backscatter signal level from the sea surface²¹. This increases signal strength in the VV (vertical-vertical) channel making it more effective for detecting oceanic features. Since most of the space borne SAR systems available today have a moderate noise floor, the cross-polarization (HV or VH) channels have not been used for oceanic feature detection. The SAR image acquired on 13th March 2024, shows the presence of two eddy features, both of which was subset and ellipsoid corrected for further preprocessing as shown in Fig. 2.

Global Sea Level Anomaly (SLA) data is freely distributed by (AVISO LAS; http://www.aviso.altimetry.fr) at a daily temporal resolution and a 0.25° horizontal resolution. These data have been effectively utilized in a variety of mesoscale eddy and monsoon studies. The surface geostrophic currents for 13th March 2023 are derived from this dataset.

Copernicus is the Earth observation component of the European Union's Space programme and it provides chlorophyll a data from satellite Earth Observation (https://cds.climate.copernicus.eu/cdsapp#!/dataset/satellite-ocean-colour?tab=form). Chlorophyll a is a green pigment and the most prevalent photosynthetic pigment in both terrestrial and marine photosynthetic organisms. As an indicator of phytoplankton abundance, and therefore the base of the marine food web, chlorophyll a concentration is recognized as an Essential Climate Variable. Oceanic chlorophyll a is usually measured in units of mg m^{-3} . The data has a resolution of 4 km x 4 km and is available on a daily basis.

The initial image pre-processing like radiometric calibration, ellipsoid correction is done using Sentinel Application Platform (SNAP). The images are then subset for speckle filtering using various filters like Lee filter, Frost filter and Boxcar filter. A performance matrix based on single speckle index is done in order to choose the best filtered output using speckle index.

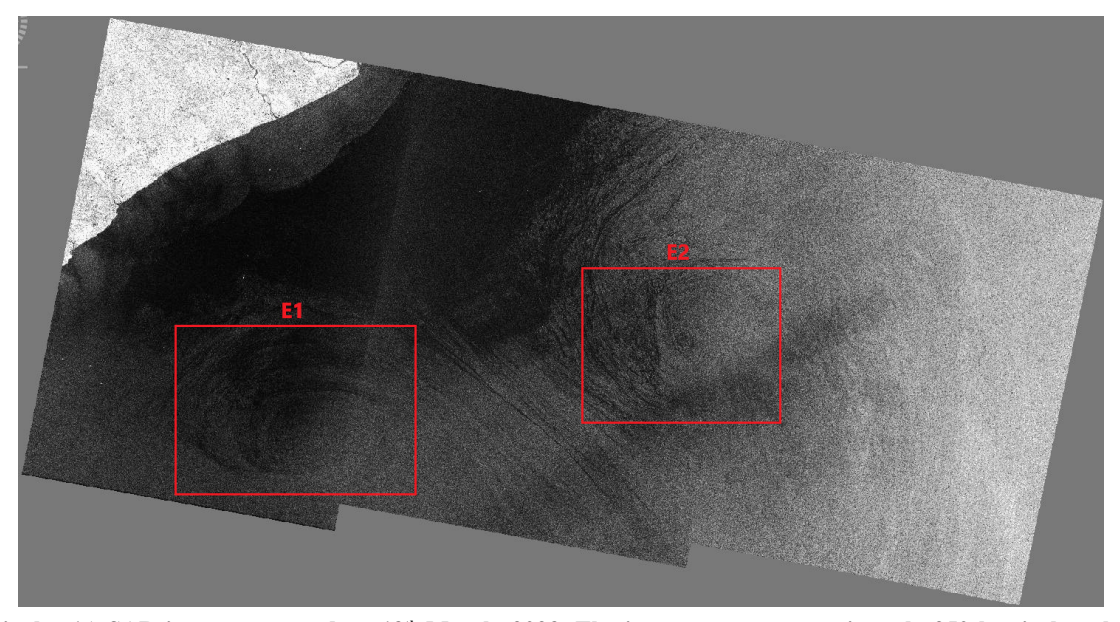


Figure 2. Sentinel – 1A SAR image, captured on 13th March, 2023. The image covers approximately 250 km in length and 120 km in width, where one pixel is 10 m x 10 m. The red boxes mark out the subsets of Eddy1 (E1) and Eddy2 (E2) respectively.

Adaptive thresholding is done in order to further extract the eddy features.

Ideally the geostrophic currents are computed and the eddy centres are overlaid on it to understand its characteristics. The same is done using chlorophyll *a* data and is compared with the SAR image data.

2.1 Despecking of SAR Images

Satellite images are usually degraded by noise during image acquisition and transmission process. Speckle is a signal dependent granular noise which occurs in all active coherent imaging systems. It reduces the quality of the images which makes processes such as segmentation and classification difficult. The filters selected are standard despeckle filters used by researchers for despeckling SAR images of ocean surfaces. The filters considered in this study are Lee filter, Frost filter and Boxcar filter²²⁻²⁴.

2.2.1 Lee Filter

Lee filter is one of the despeckle filters that reduces SAR speckle based on local statistics. It is computed by applying minimum mean square error (MMSE). The equation is as follows:

$$\hat{I}(x,y) = \overline{I}(x,y) + W(x,y) * \left[I(i,j) - \overline{I}(x,y) \right] \tag{1}$$

where, $\hat{I}(x,y)$ is the filtered image, I(i,j) is the centre pixel and $\bar{I}(x,y)$ is the mean of the window. W(x,y) is the weight function and is given by,

$$W(x,y) = \frac{\sum \sum \sigma_k^2(x,y)}{\sum \sum (\sigma_k^2 + \sigma^2)}$$
 (2)

where, $\sigma_k^2(x, y)$ is variance of pixels in kernel/window and $\sigma^2(x, y)$ is the variance of image.

2.2.2 Frost Filter

Frost filter is a Bayesian method in spatial domain which was designed by making assumptions on the statistical properties of reflectivity and speckle.

It works on preserving the edges while supressing the noise. The damping factor is exponential which is the key factor in smoothness of the filter. When the damping factor is small the image tends to be smoother²⁵.

$$\hat{I}(i,j) = \sum_{s} \sum_{h} P_{sh} m_{sh} / \sum_{s} \sum_{h} m_{sh},$$

$$m_{sh} = e^{-KC_I^2 d_{sh}}$$
(3)

where, (i, j) is location of the current pixel, $\hat{I}(i,j)$ denotes the output of the filter, P_{sh} denotes the value of the pixels among the window centered at (i, j), K (K>0) is the tuning factor, C_I is the coefficient of the variation that is defined by the ratio of the sample standard deviation to sample mean and d_{sh} is the distance between any pixel in current window to the centre pixel.

2.2.3 Boxcar Filter

It is a type of low-pass filter which removes the noise with a high frequency spectrum as well as smoothing the details such as the edges and points. It works by replacing each pixel value with the average of its neighbouring pixels within a defined window. Its equation is as follows:

$$X(i,j) = 1/N \sum Y(i,j) \tag{4}$$

where, X(i,j) represents the estimated pixel value constructed by computing the sample mean over each pixel neighbourhood and Y(i,j) is the original noisy image.

2.2 Computing the Performance Matrix

Speckle index is a means of measuring speckle reduction. It is defined as follows:

$$c_{si} = \frac{\sigma}{\mu} \tag{5}$$

where, σ is the standard deviation and μ is the mean of the intensity of the image.

2.3 Adaptive Thresholding of SAR Images

Adaptive threshold is a dynamic method used in image processing to segment an image by varying the threshold value across different regions of the image. This technique is particularly useful in SAR image processing due to the presence of varying intensities and noise levels throughout the image. It is particularly helpful to reduce the noise impact, segmentation and enhance edge detection.

Adaptive thresholding is done for the best filtered image to enhance the eddy intensity pattern and also improve the detection of eddy boundaries by adjusting to local variation, thus providing more precise and continuous boundaries compared to global thresholding methods.

2.4 Geostrophic Currents

The surface geostrophic currents are estimated using the following Eqn.:

$$u = \frac{-g}{f} \frac{\partial \zeta}{\partial y} \tag{6}$$

$$v = \frac{g}{f} \frac{\partial \zeta}{\partial x} \tag{7}$$

where, g is the acceleration due to gravity, f is the Coriolis parameter and ζ is the Sea Surface Height Anomaly (SSHA)²⁶. The geostrophic currents are plotted and the presence of cyclonic or anticyclonic eddies are detected.

3. RESULTS

Two prominent eddies, labeled E1 and E2 (Fig. 2), are clearly visible. E1 is a cyclonic spiral eddy centered at approximately 17.66° N: 84.90° E. It is located around 60 km from the coast, with a diameter of about 50-60 km. E2 is an asymmetrical cyclonic eddy, measures roughly 40-50 km in size, with its center at 17.48° N: 83.98° E. It is situated at roughly around 110 km from the coast. The centers were estimated after geometric correction was carried out using SNAP software.

3.1 Despecking of SAR Images

A performance matrix is generated in order to find out the best filtered outputs. The filtered images of both E1 and E2 are given in Fig. 3. The Speckle Index (SI) is computed for both original image and the filtered outputs of both subsets. The Difference of SI (DSI) of original image subsets (E1 & E2)

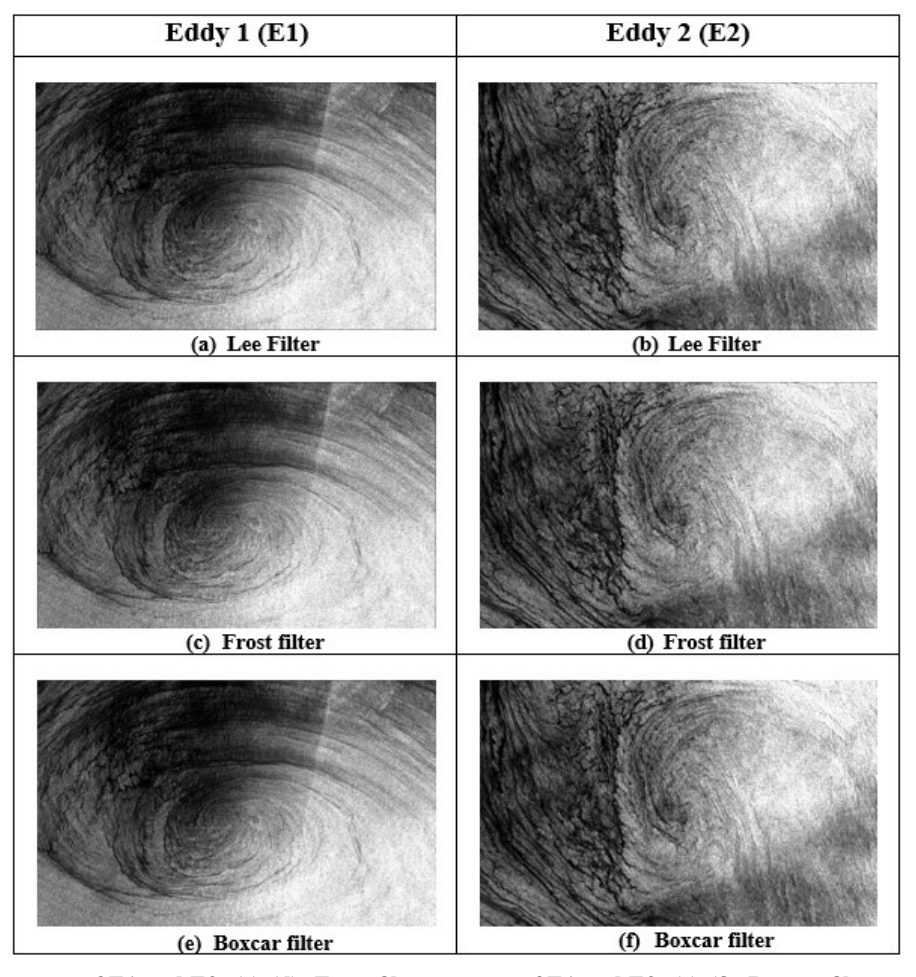


Figure 3. (a)-(b): Lee filter outputs of E1 and E2; (c)-(d): Frost filter outputs of E1 and E2; (e)-(f): Boxcar filter outputs of E1 and E2.

Table 1. Performance matrix based on the Difference of Speckle index (DSI) of E1 and E2

Filters	DSI(E1)	DSI(E2)
Lee filter	0.1686	0.1892
Frost filter	0.1660	0.1833
Boxcar filter	0.1723	0.1929

and their respective filtered outputs are calculated as shown in Table 1.

The DSI between the original image and each filtered output is computed as a performance matrix, which implies that greater the DSI value less speckle is in the image. It can be observed from Table 1 that Boxcar filter has the largest DSI value in the case of both E1 and E2. Hence Boxcar filtered outputs are chosen for further analysis.

3.2 Adaptive Threshold

Adaptive thresholding is carried out on the despeckled images to visualize the flow of currents. It helps in the interpretation of the characteristics of eddies under study.

The selected image is processed and for each pixel in the image, a threshold is calculated based on the the local mean intensity in the local neighbourhood. If the pixel value is below the threshold it is set to the background value, otherwise it assumes foreground value. The eddy features are enhanced

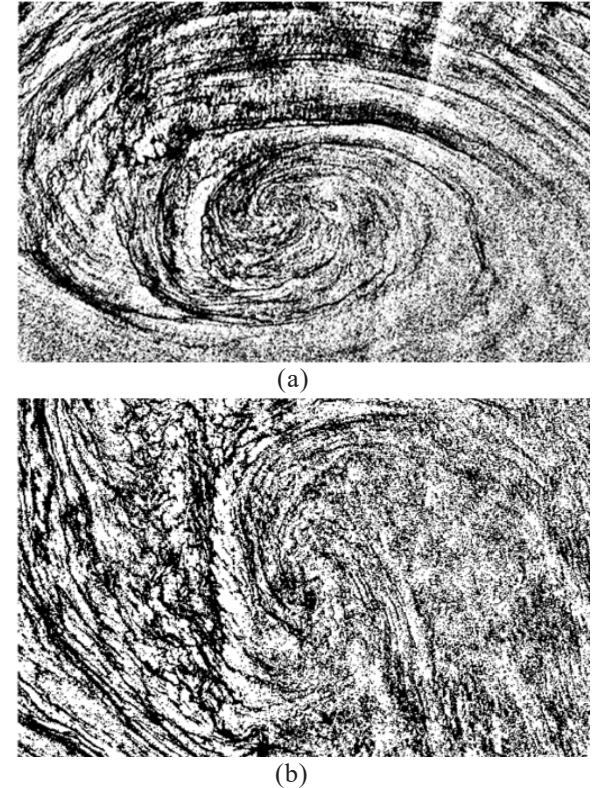


Figure 4. (a) Adaptive threshold output of Eddy1; and (b) Adaptive threshold output of Eddy2.

and boundary detection becomes smoother with continuous boundary lines.

3.3 Geostrophic Currents

The distribution of geostrophic currents derived from SLA near the North-Western BoB on March 13, 2023, is depicted in Fig. 5. Within the delineated black box, there is a pronounced SLA minimum of 22 cm, located approximately at 18° N, 85° E, which corresponds to the region of SAR imagery acquisition. The observed SLA minimum and the associated anti-clockwise circulation are indicative of a cyclonic eddy. Southward of this cyclonic feature, a dominant anticyclonic circulation is present, characterized by an SLA maximum of 45 cm around 16° N, 83.7° E. Additionally, there is a noticeable convergence of currents between the two eddies, forming an eastward-flowing current at 17.5° N. The cyclonic eddy has an approximate diameter of 100 km, whereas the anticyclonic eddy extends about 200 km into the central Bay of Bengal.

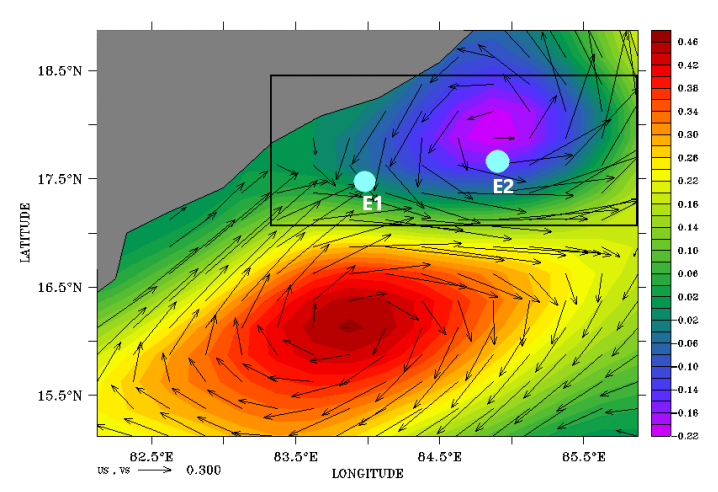


Figure 5. Sea Level Anomaly (SLA) overlaid with Geostrophic currents, near North-western BoB. The black box indicates the SAR image footprint. The cyan blue circles mark out the eddy centers of E1 and E2.

The two cyan blue markers labeled E1 and E2 represent the centers of the eddies detected from the SAR image. E1 is situated at the convergence point of the currents generated by both eddies. E1 exhibits a distinct spiral pattern and is cyclonic, suggesting a high possibility of its formation due to the unstable perturbations in the larger geostrophic flows. Such instabilities can induce frontogenesis, causing the breakup and curling of flows, which subsequently form smaller cyclonic spiral eddies⁶.

E2 is located further north, with its center in close proximity to the SLA minimum, suggesting that it is part of the larger cyclonic eddy. E2 exhibits an asymmetrical pattern, complicating the detection of its boundaries, as it may be larger than estimated from the SAR imagery.

The chlorophyll distribution at the North-Western BoB on 13th March 2023 is given in Fig. 6. This data confirms that both features are cyclonic circulations, as indicated by the local increase in chlorophyll concentration, which is visible as green patches around the marked eddy centers. The pronounced south-eastward flow is also apparent from the chlorophyll data, which corresponds well with the geostrophic current data.

From Fig. 6, the two cyan blue dots labeled E1 and E2 represent the eddy centers identified from the SAR image, and the black box demarcates the region where the SAR image was captured. Below the 18° N latitude, there is a notable lack of chlorophyll -a, while a local high in chlorophyll -a production is observed north of this latitude. This distribution aligns well with the cyclonic and anticyclonic circulations depicted in Fig. 5.

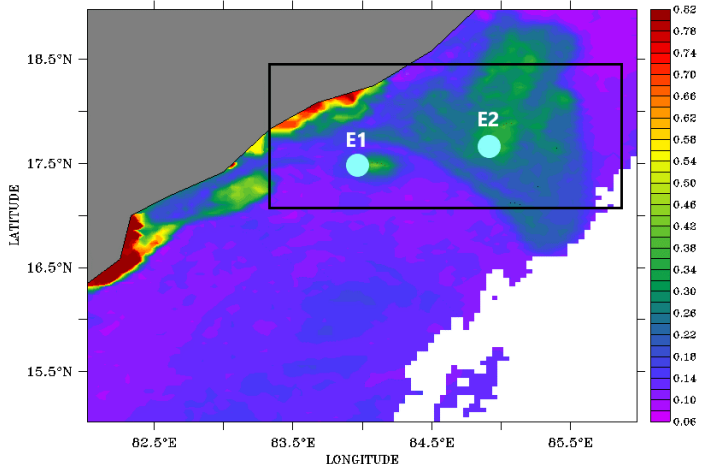


Figure 6. Chlorophyll -a distribution of western BoB on 13th March 2023, with eddy centers E1 and E2 marked as cyan blue circles. The black box marks out the SAR image footprint.

The local increase in chlorophyll -a production near E1 and E2 confirms that both eddies are cyclonic. A distinct circular patch near E1 matches well with the cyclonic spiral eddy. Additionally, the chlorophyll a data reveals a distinct current pattern, with high chlorophyll a concentrations (green) and low concentrations (purple) marking the interface between the two eddies. The chlorophyll a production near E2 spans a larger area, corroborating that it is a larger eddy than indicated by the SAR image.

4. DISCUSSION AND CONCLUSIONS

The integration of SAR, SLA and chlorophyll-a data provides a comprehensive understanding of the geostrophic currents and eddy formations in the North-western BoB during the month of March, 2023. The detection of two prominent eddies, E1 and E2 (Fig. 2), using SAR images and their verification using chlorophyll-a data highlights the intricate dynamics of cyclonic and anticyclonic circulations in this region.

The BoB is characterized by high stratification and regular influxes of freshwater from rivers, complicating the identification and categorization of minor variations using Sea Surface Temperature (SST). Consequently, these features may not exhibit the typical temperature variations associated with eddies, underscoring the importance of a multi-sensor approach. By utilizing ocean colour data and geostrophic currents derived from SLA, these oceanographic features are validated.

The geostrophic currents derived from altimetry data failed to detect eddy E1, despite its size of approximately 50

km to 60 km, which is within the expected resolution of satellite altimetry (25 km). There is also a significant difference in the eddy centers of E2 from the SAR image and the SLA data which is evident from Fig. 5. The discrepancy between the centers of E2 may be attributed to the difference in resolutions of the datasets. Its asymmetrical pattern complicates boundary detection, suggesting that it may be larger than estimated from SAR imagery. The chlorophyll-*a* data, with a resolution of 4 km, provides clear insights and substantiate the presence and extent of these eddies. It also captured the steady south-eastward flow between the cyclonic and anticyclonic circulations.

One drawback is that an ambient wind condition (<6m/s) is required for the eddy formation to be visible in SAR images. The eddy detection from SAR images becomes difficult during strong winds as the surface film may get disrupted.

The use of SAR imagery has been pivotal in identifying and characterizing the cyclonic eddies, E1 and E2, in the North-Western BoB. The study emphasizes the limitations of altimetry data for detection of sub-mesoscale eddies and demonstrates the importance of high-resolution SAR data in capturing detailed oceanographic features. The combined analysis of SAR and chlorophyll-*a* data provides a comprehensive view of the interactions between cyclonic and anticyclonic circulations. Future research shall focus on the evolution and impact of eddies on regional marine ecosystems and coastal processes.

REFERENCES

- Robinson AR. Overview and summary of eddy science. InEddies in marine science 1983 (pp. 3-15). Berlin, Heidelberg: Springer Berlin Heidelberg.
- 2. Stuhlmacher A, Gade M. Statistical analyses of eddies in the Western Mediterranean Sea based on Synthetic Aperture Radar imagery. Remote Sensing of Environment. 2020 Dec 1;250:112023.
- Gade M, Byfield V, Ermakov S, Lavrova O, Mitnik L. Slicks as indicators for marine processes. Oceanography. 2013 Jun 1;26(2):138-49.
- Grooms I, Zanna L. A note on 'Toward a stochastic parameterization of ocean mesoscale eddies'. Ocean Modelling. 2017 May 1;113:30-3.
- 5. Fedorov KN. The physical nature and structure of oceanic fronts. Berlin: Springer-Verlag; 1986 Jan 1.
- 6. Eldevik T, Dysthe KB. Spiral eddies. Journal of Physical Oceanography. 2002 Mar;32(3):851-69.
- 7. Thomas L, Ferrari R. Friction, frontogenesis, and the stratification of the surface mixed layer. Journal of Physical Oceanography. 2008 Nov;38(11):2501-18.
- McWilliams JC, Fox-Kemper B. Oceanic wave-balanced surface fronts and filaments. Journal of Fluid Mechanics. 2013 Sep;730:464-90.
- 9. Chelton DB, Schlax MG, Freilich MH, Milliff RF. Satellite measurements reveal persistent small-scale features in ocean winds. science. 2004 Feb 13;303(5660):978-83.
- Cheng YH, Ho CR, Zheng Q, Kuo NJ. Statistical characteristics of mesoscale eddies in the North Pacific derived from satellite altimetry. Remote Sensing. 2014 Jun 5;6(6):5164-83.

- 11. Da Silva, J. C. B., et al. Role of surface films in ERS SAR signatures of internal waves on the shelf: 1. Short-period internal waves. Journal of Geophysical Research: Oceans 103.C4 1998, 8009-8031.
- 12. Clemente-Colón P, Yan XH. Low-backscatter ocean features in synthetic aperture radar imagery. Johns Hopkins APL Technical Digest. 2000 Jan 1;21(1):116-21.
- 13. Shankar D, Vinayachandran PN, Unnikrishnan AS. The monsoon currents in the north Indian Ocean. Progress in oceanography. 2002 Jan 1;52(1):63-120..
- Paul, R. & Dube, S. Bay of Bengal: An overview Springer (2015).
- Shankar, D. & Shetye, S. Seasonal Variability of the East India Coastal Current. Journal of Geophysical Research.1997, 102.C6, 12977-12988.
- 16. Sikka, D. R. & Suresh, N. Monsoon Precipitation in the Bay of Bengal. Climate Dynamics, 2010, 35(4), 809-821.
- 17. Schott FA, McCreary Jr JP. The monsoon circulation of the Indian Ocean. Progress in Oceanography. 2001 Jan 1;51(1):1-23.
- 18. Vialard, J. & Delecluse, P. The East Indian Coastal Current and its variability. Deep-sea Research Part-1: Oceanographic Research Papers, 45(5), 945-967.
- 19. Vidya PJ, Kumar SP. Role of mesoscale eddies on the variability of biogenic flux in the northern and central Bay of Bengal. Journal of Geophysical Research: Oceans. 2013 Oct;118(10):5760-71.
- Jyothibabu R, Madhu NV, Maheswaran PA, Jayalakshmy KV, Nair KK, Achuthankutty CT. Seasonal variation of microzooplankton (20–200 μm) and its possible implications on the vertical carbon flux in the western Bay of Bengal. Continental Shelf Research. 2008 Apr 1;28(6):737-55.
- 21. Benes R, Riha K. Medical image denoising by improved Kuan filter. Advances in Electrical and Electronic Engineering. 2012 Mar 1;10(1):43.
- Zhu J, Wen J, Zhang Y. A new algorithm for SAR image despeckling using an enhanced Lee filter and median filter. In2013 6th International congress on image and signal processing (CISP) 2013 Dec 16 (Vol. 1, pp. 224-228). IEEE.
- Frost VS, Stiles JA, Shanmugan KS, Holtzman JC. A model for radar images and its application to adaptive digital filtering of multiplicative noise. IEEE Transactions on pattern analysis and machine intelligence. 1982 Mar(2):157-66.
- Lopes A, Nezry E, Touzi R, Laur H. Maximum a posteriori speckle filtering and first order texture models in SAR images. In10th annual international symposium on geoscience and remote sensing 1990 May 20 (pp. 2409-2412). Ieee.
- 25. Sun Z. Research on MMSE despeckling algorithm for SAR image. Comput. Appl. Softw.. 2012;29(7):18-21.
- Stewart RH. Introduction To Physical Oceanography, Department of Oceanography, Texas A & M University Editions, 351 pp.

ACKNOWLEDGEMENT

The authors would like to acknowledge Director NPOL for the support and encouragement in carrying out the work. This work has been carried out as part of technical activities pertaining to Project NPL 256.

CONTRIBUTORS

Ms Maria Sansanna obtained her Masters in Oceanography and MTech in Ocean Technology from Cochin University of Science and Technology, Kochi, Kerala. She is a Project Associate at DRDO-NPOL, Kochi. Her areas of research include: Oceanic eddies, synthetic aperture radar images.

Contribution in the present study: Data collection, implementation of methodology and drafting of manuscript.

Dr Lekshmi S. obtained her PhD in Computer Science from University of Kerala and working as a Scientist at DRDO-NPOL, Kochi. Her areas of research include: Image processing, synthetic aperture radar.

Contribution in the current study: Conception and design.

Dr P.A. Maheswaran obtained his PhD in Oceanography from Cochin University of Science and Technology. Currently working as a Scientist at DRDO-NPOL, Kochi, Kerala. His areas of research include: Detection of oceanic eddies.

In the present study he has done analysis and interpretation.

Mr Praveen Naresh obtained his Masters in Meteorology and MTech in Atmospheric Science from Andhra University, Visakhapatnam, India. He is working as a Scientist at DRDO-NPOL, Kochi, Kerala. His Research Interest are Satellite image processing, synthetic aperture radar.

In the current study, he done validation and review of manuscript.